Optics Letters

Ultrafast resonant exciton–plasmon coupling for enhanced emission in lead halide perovskite with metallic Ag nanostructures

Yuxiang Tang,[1] Yanbin Zhang,[2] Fan Cao,[1] Yizhen Sui,[1] Xiang'ai Cheng,[1] Lei Shi,[2,4] and Tian Jiang[1,3,*]

[1]College of Advanced Interdisciplinary Studies, National University of Defense Technology, Changsha 410073, China
[2]Key Laboratory of Micro- and Nano-Photonic Structures (Ministry of Education), and State Key Laboratory of Surface Physics, Department of Physics, Fudan University, Shanghai 200433, China
[3]Beijing Institute for Advanced Study, National University of Defense Technology, 100000 Beijing, China
[4]e-mail: lshi@fudan.edu.cn
*Corresponding author: tjiang@nudt.edu.cn

Received 25 April 2022; revised 1 July 2022; accepted 10 July 2022; posted 11 July 2022; published 28 July 2022

Integrating metal halide perovskites onto plasmonic nanostructures has recently become a trending method of enabling superior emissive performance of perovskite nanophotonic devices. In this work, we present an in-depth study on the spontaneous emission properties of hybrid systems comprising $CsPbBr_3$ nanocrystals and silver nanostructures. Specifically, a 5.7-fold increment of the photoluminescence (PL) intensity and a 1.65-fold enhancement of the PL relaxation rate is attained when the transition energy of $CsPbBr_3$ is spectrally resonant with the oscillational frequency of Ag nanodisks (NDs), which is attributed to the intense exciton–plasmon coupling-induced Purcell effect. Furthermore, a 540-fs ultrafast energy transfer from the $CsPbBr_3$ excitons to Ag plasmons is revealed by femtosecond pump-probe experiments, suggesting the key mechanism responsible for the Purcell-enhanced radiative emission. Our finding offers a unique understanding of the enhanced emissive behavior in the plasmon-coupled perovskite system and paves the way for further applications.

https://doi.org/10.1364/OL.461926

The study of advanced nanophotonics based on all-inorganic lead halide perovskites $CsPbX_3$ (where X = Cl, Br, or I) has been the mainstream of research in both fundamental physics and device applications over the last few years [1–3], owing to their wide tunable bandgap, robust excitons (i.e., large absorption coefficient and strong luminescent efficiency), high carrier mobility, and low cost [4]. These excellent optoelectronic properties make them highly promising candidates for the next-generation light source, especially for on-chip integrated light emitting diodes (LEDs) [5–7] and nanolasers [8–10]. Despite the great advantages, there is still much room for improvement in the emission brightness and emission rate of perovskite-based devices in order to satisfy the ultimate demands of practical applications. Therefore, it is important and indispensable to achieve active manipulation on the spontaneous emission behavior of the perovskite emitters in the nanoscale.

The coupling of all-inorganic lead halide perovskite emitters to optical resonators, including dielectric microcavities and plasmonic nanocavities, has been proved to be an extremely promising means of improving the photoluminescence (PL) emission properties of perovskite [11–13]. This is because not only can the pump light excitation rate and PL signals collection efficiency can be ameliorated by the presence of cavities [14,15], but also the radiative rate of emitters can be significantly enhanced via the strongly modified local density of photonic states, which is often referred to as the Purcell effect [16,17]. Nevertheless, a thorough understanding of the physical process of the Purcell effect in these hybrid perovskite-based nanophotonic devices remains elusive, especially in the case of plasmonic nanocavity-based systems, where the coupling interaction between excitons and plasmons usually determines the Purcell effect [18]. Consequently, it is of foremost importance to figure out how the Purcell-enhanced radiative emission process occurs through exciton–plasmon coupling in these metallic nanostructure-based perovskite systems, as this will help us better acknowledge the intrinsic physical nature of the Purcell effect and thus promote the development of halide perovskite nanophotonic devices.

In this Letter, we systematically investigate the spontaneous emission of a resonant coupled heterostructure consisting of $CsPbBr_3$ nanocrystal film and patterned Ag nanodisks (NDs) via steady-state and time-resolved spectroscopy. Specifically, the PL emission intensity and emission rate of the hybrid system are both effectively enhanced due to the Purcell effect. Then, this resonant exciton–plasmon coupling-governed Purcell effect was further explored by using femtosecond pump-probe measurements, revealing an ultrafast Förster-like energy transfer from the $CsPbBr_3$ to Ag ND with a characterized time of ~540 fs.

The schematic illustration of the Ag ND-$CsPbBr_3$ hybrid system studied in our work is shown in Fig. 1(a). Specifically, well-defined silver nanodisk arrays with a height of 30 nm were first prepared and patterned directly on the top of a precleaned quartz substrate via electron-beam evaporation followed by a lift-off process. Then, a ~30 nm alumina (Al_2O_3) dielectric spacer

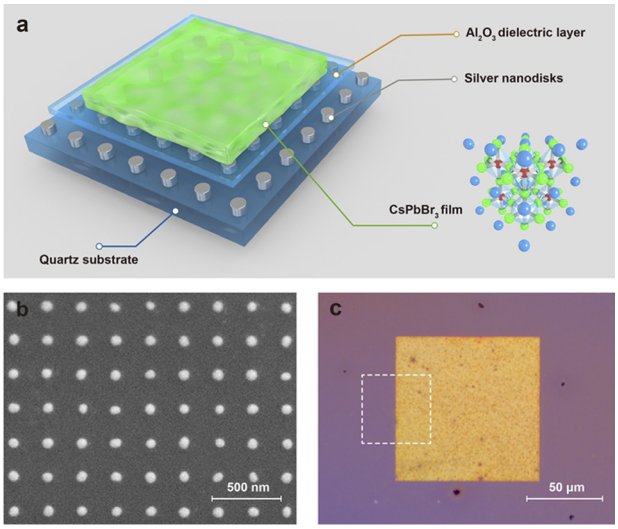

Fig. 1. (a) Schematic diagram of the Ag ND-$CsPbBr_3$ hybrid system. (b) Scanning electron microscopy image of the Ag ND structure. (c) Optical microscopy image of the fabricated Ag ND-$CsPbBr_3$ sample. The white dashed box is the place where PL mapping was conducted.

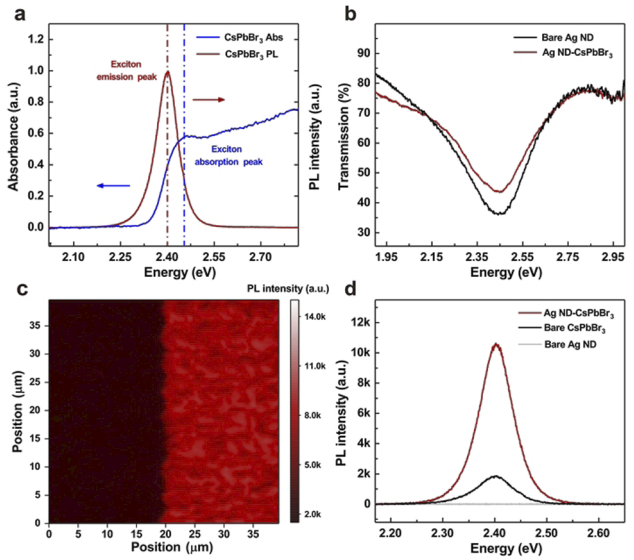

Fig. 2. (a) Absorption and PL spectra of bare $CsPbBr_3$ nanocrystals used in our work. (b) Transmission spectra of the fabricated bare Ag ND and hybrid Ag ND-$CsPbBr_3$ sample. (c) PL mapping image obtained from the white dashed box area in Fig. 1(c) probed at 2.40 eV. (d) PL spectra comparison of the bare Ag ND, bare $CsPbBr_3$, and hybrid Ag ND-$CsPbBr_3$. All the PL experiments carried here are stimulated by a 405-nm pulsed laser with a low excitation fluence of 1 μj cm^{-2}.

formed by the atomic layer deposition technique was utilized to passivate the Ag NDs, thus avoiding charge transfer quenching from the direct contact between the metallic nanostructure and perovskite. Finally, a $CsPbBr_3$ nanocrystals dilute solution in toluene (10 mg/mL) was dispersed onto the entire nanostructured sample surface via the spin-coating method (2000rpm for 1 min), resulting in a thin perovskite film with a thickness of ~50 nm. To prevent unwanted degradation during the testing, all samples were encapsulated by a 200-nm thick layer of polymethyl methacrylate (PMMA A4, spin coating at 4000 rpm for 40 s). Figure 1(b) shows the scanning electron microscopy image of the fabricated Ag ND, in which the lattice periodicity and diameter of the nanodisk were designed to be 250 nm and 60 nm, respectively. Moreover, the optical microscopy of the hybrid sample is further presented in Fig. 1(c), indicating the good morphology and quality of our sample.

Figure 2(a) characterizes the optical absorption and PL spectra of the $CsPbBr_3$ nanocrystal investigated in our study. The clear excitonic absorption peak at 2.45 eV and narrow excitonic emissive peak at 2.40 eV (with full width at half-maximum of ~76 meV) imply the strong oscillator strength and stable nature of the $CsPbBr_3$ exciton at room temperature, which is beneficial for realizing robust resonant exciton–plasmon coupling. The transmission spectrum of the bare Ag ND is further recorded as the black solid line in Fig. 2(b). A prominent and broadband spectral dip originated from the localized surface plasmon resonance (LSPR) is observed to emerge at 2.45 eV, providing a reasonable resonant match with the energic transition of the $CsPbBr_3$ exciton. The transmission spectrum of the integrated Ag ND-$CsPbBr_3$ is displayed as the red solid line in Fig. 2(b) and demonstrates a slightly enhanced transmission at resonance energy position compared with the bare Ag ND, which evidences the interplay between $CsPbBr_3$ and Ag ND. Specifically, the simultaneous spectral and spatial location overlap of the $CsPbBr_3$ and Ag ND elements guarantees an effective near-field energy exchange between exciton and plasmon, and the absence of Rabi splitting in the transmission spectrum, suggests the exciton–plasmon interaction in our system is in the weak coupling regime [19], in which a modified emission feature of the $CsPbBr_3$ emitter might be expected. Therefore, a steady-state PL experiment under 405 nm (i.e., 3.06 eV) pulsed laser excitation was first employed to study the emission property of the coupled Ag ND-$CsPbBr_3$ sample. Figure 2(c) presents a typical PL mapping result scanning from the white dashed area marked in Fig. 1(c) and a significant PL enhancement is clearly found when the $CsPbBr_3$ is coupled with the Ag ND. The average PL spectra of the bare $CsPbBr_3$ and hybrid Ag ND-$CsPbBr_3$ are further acquired and compared in Fig. 2(d), revealing a biexciton state-free symmetric Lorentzian line shape [20,21] and a broad intensity enhancement as considerable as ~5.7-fold. Notably, the PL spectrum of the bare Ag ND is also included in Fig. 2(d) and shows no contribution to the overall PL signal, proving that the improved emission performance of the hybrid system is derived from the efficient interplay between the $CsPbBr_3$ exciton and Ag ND plasmon. Basically, three types of exciton–plasmon interaction mechanisms can lead to enhanced PL behavior in light emitters: (i) the intense local plasmonic electromagnetic field enhanced pump light absorption; (ii) the directional emission improved collection efficiency; (iii) the Purcell effect increased spontaneous emission rate. In our system, neither pump light absorption enhancement nor collection efficiency improvement are intuitively the main factors responsible for the PL enhancement as the excitation laser energy is far from the plasmon resonance energy and the detected angular range of the used objective (LEICA, N PLAN EPI 100×, NA = 0.85) is wide enough to collect most of the PL signals. As a result, we assume the exciton–plasmon coupling-governed Purcell-enhanced radiative emission is the primary reason for the PL intensity boosting of our sample.

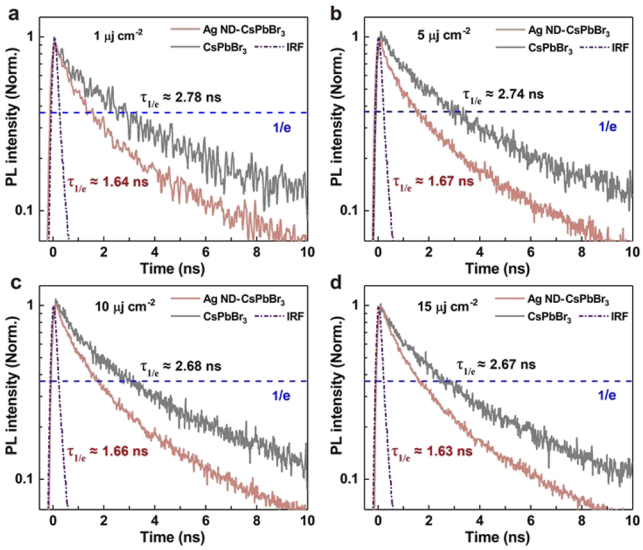

Fig. 3. Comparison of normalized PL decay from the bare $CsPbBr_3$ (black) and hybrid Ag ND-$CsPbBr_3$ (red) samples at 2.40 eV under different excitation fluences. Blue dashed lines represent the 1/e position of normalized PL intensity, which provides guidance in determining the exact value of $\tau_{1/e}$. The gray lines stand for the instrumental response function (IRF) of the TCSPC with a full width at half-maximum of ~300 ps.

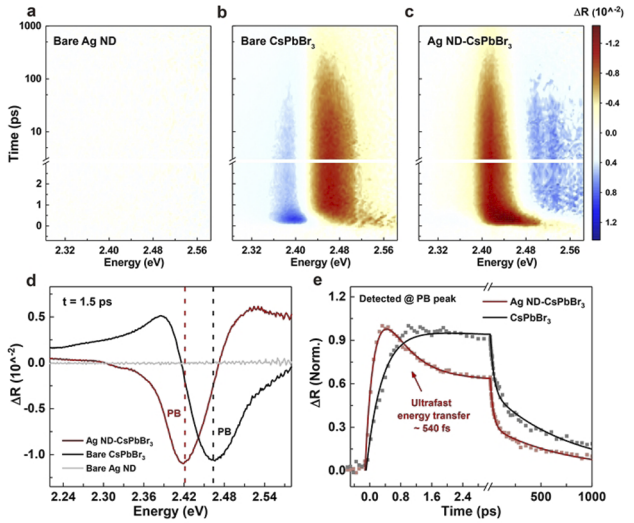

Fig. 4. Time-resolved differential reflection spectra of (a) bare Ag ND, (b) bare $CsPbBr_3$, and (c) hybrid Ag ND-$CsPbBr_3$ excited under 7.5 μj cm^{-2}. (d) Comparison of the extracted ΔR spectra of Ag ND (gray), $CsPbBr_3$ (black), and Ag ND-$CsPbBr_3$ (red) at 1.5 ps. (e) ΔR kinetics of $CsPbBr_3$ (black) and Ag ND-$CsPbBr_3$ (red) monitored at the PB peaks. Solid lines are the multi-exponential fitting results.

To directly verify the observation of the Purcell effect, time-resolved PL measurements were performed for both the $CsPbBr_3$ and Ag ND-$CsPbBr_3$ sample by utilizing the time-correlated single-photon counting (TCSPC) technique under 405 nm picosecond-pulsed laser irradiation (80 ps, 20 Mhz). As shown in Fig. 3, we notice the PL dynamics of the Ag ND-$CsPbBr_3$ sample demonstrate a similar faster decay than that of the isolated $CsPbBr_3$ for a large range of pump fluences, which proves that the accelerated PL relaxation is not affected by the fluence-dependent exciton–exciton annihilation interactions [22] and thus indeed originate from the Purcell effect. To further quantitively describe the PL dynamics, we defined the lifetime $\tau_{1/e}$ in the formula $I(t=\tau_{1/e})=I(t=0)/e$ as the effective lifetime of PL decay in our work, where $I(t=\tau_{1/e})$ represents the PL signal at $t=\tau_{1/e}$ and its intensity is 1/e times the initial PL intensity $I(t=0)$. Correspondingly, the extracted numerical results of $\tau_{1/e}$ are listed in detail and compared in Fig. 3, and a substantial decline of $\tau_{1/e}$ can be found when the $CsPbBr_3$ is coupled to the Ag ND. Taking the ratio of $\tau_{1/e}$ in the bare $CsPbBr_3$ case to that in the hybrid Ag ND-$CsPbBr_3$ case, we attain an average PL relaxation rate enhancement factor of 1.65 ± 0.06, confirming the enhancement of spontaneous radiative emission. It should be noted that this PL relaxation rate enhancement factor can be exploited to approximately reflect the magnitude of the Purcell factor whenever the radiative recombination process in PL dynamics outcompetes the nonradiative recombination process.

Unfortunately, a more subtle photophysical process of the Purcell effect cannot be explored further here due to the limited time resolution of the TCSPC, which hinders the understanding of how the exciton–plasmon coupling dominates the Purcell-enhanced radiative emission.

Additional insights into the exciton–plasmon coupling-governed Purcell-enhanced radiative emission in the Ag ND-$CsPbBr_3$ system are provided by transient differential reflection (ΔR) spectroscopy. In the experiment, a femtosecond pump pulse (≈100 fs, 3.10 eV, 1 kHz) was employed to excite the sample, and the induced reflection changes (i.e., ΔR) were subsequently detected by a followed white light continuum probe pulse with a controllable time delay. Figures 4(a)–4(c) show the 2D pseudo-color maps of the measured ΔR signals for the bare Ag ND, bare $CsPbBr_3$, and hybrid Ag ND-$CsPbBr_3$. As can be seen, both the spectral and temporal behaviors of ΔR signals change dramatically from the uncoupled case to the coupled case. For a clearer inspection, the ΔR spectra of Ag ND, $CsPbBr_3$, and Ag ND-$CsPbBr_3$ at 1.5 ps are carefully compared in Fig. 4(d). The bare Ag ND shows no signals, while the $CsPbBr_3$ and Ag ND-$CsPbBr_3$ show similar but antisymmetric signals. This fact indicates that the optical response of the coupled system is not a simple superposition of the isolated system, and it is the intense exciton–plasmon coupling-induced Fano interference that makes the line shape of ΔR spectrum of the $CsPbBr_3$ system transform into the antisymmetric one of the Ag ND-$CsPbBr_3$ system [23,24].

To access the characteristic time of the exciton–plasmon coupling, ΔR kinetics of the $CsPbBr_3$ and Ag ND-$CsPbBr_3$ at photoinduced bleaching (PB) peaks are further analyzed by a multi-exponential function in Fig. 4(e). Related fitting results are displayed in Table 1. One prominent finding is that an extra-fast decay channel with a lifetime (τ_2) of ~0.54 ps appears in the kinetics of Ag ND-$CsPbBr_3$, while it is absent in the case of bare $CsPbBr_3$. We attribute this rapid decay to the ultra-fast nonradiative energy transfer from the $CsPbBr_3$ exciton to the Ag ND plasmon, which is conducted through a Förster-like dipole–dipole interaction [25]. Meanwhile, this fast decay also effectively competes with the hot carrier cooling process, leading to a faster exciton build-up time (τ_1) in Ag ND-$CsPbBr_3$. The lifetimes of the slow decays (τ_3, τ_4) are almost same for both the $CsPbBr_3$ and Ag ND-$CsPbBr_3$ systems, reflecting the Auger and trap-assisted nonradiative recombination of the excess excitons.

Table 1. Fitting Parameters of the Time-Resolved ΔR Signal

	$CsPbBr_3$	Ag ND-$CsPbBr_3$
τ_1 (rise)	0.40 ps	0.28 ps
τ_2 (fast decay)	N/A	0.54 ps
τ_3 (slow decay)	35.0 ps	31.0 ps
τ_4 (slow decay)	769 ps	729 ps

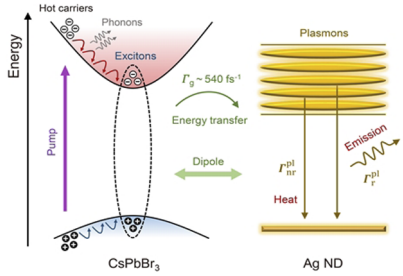

Fig. 5. Schematic of the mechanism of Purcell-enhanced radiative emission in the studied Ag ND-$CsPbBr_3$ hybrid system.

Unfortunately, the radiative lifetimes of the systems are too long to be observed here due to the limited time window. Overall, the Purcell-enhanced radiative emission process in our Ag ND-$CsPbBr_3$ sample can be schematically understood as multiple stages shown in Fig. 5. First, the photogenerated hot carriers cool down to the exciton band edge via phonon dissipation. Then, the formed excitons rapidly deliver their energy to plasmons at a rate of Γ_g (540 fs^{-1}) via exciton–plasmon coupling-governed ultrafast energy transfer. Finally, the excited plasmons behave like an antenna and undergo radiative and nonradiative damping at rates of $\Gamma^{pl}{}_r$ and $\Gamma^{pl}{}_{nr}$, respectively, resulting in an ultimate spontaneous radiative emission rate of $\Gamma_g * \Gamma^{pl}{}_r/(\Gamma^{pl}{}_r+\Gamma^{pl}{}_{nr})$ for the Ag ND-$CsPbBr_3$ system [25].

In summary, we have carried out an in-depth experimental study on the Purcell-enhanced radiative emission in a hybrid structure comprising Ag NDs and $CsPbBr_3$. By applying femtosecond pump-probe measurements, we reveal a 540-fs energy transfer from $CsPbBr_3$ to Ag ND via intense resonant exciton–plasmon coupling. This ultrafast energy transfer greatly impedes the nonradiative electron–phonon and exciton–exciton Auger loss in $CsPbBr_3$ and effectively increase the exciton spontaneous emission rate, resulting in a brighter and faster luminescence of the light emitter. This work sheds new light on improving the emission properties of the perovskite, which will facilitate the development of on-chip ultrafast perovskite photonic devices.

Funding. Science and Technology Commission of Shanghai Municipality (19DZ2253000, 19XD1434600, 2019SHZDZX01); The Science and Technology Innovation Program of Hunan Province (2021RC2068); The Science Fund for Distinguished Young Scholars of Hunan Province (2020JJ2036); National Natural Science Foundation of China (62075240, 62105364).

Disclosures. The authors declare no conflicts of interest.

Data availability. Data underlying the results presented in this paper are not publicly available at this time but may be obtained from the authors upon reasonable request.

REFERENCES

1. B. R. Sutherland and E. H. Sargent, Nat. Photonics **10**, 295 (2016).
2. S. Makarov, A. Furasova, E. Tiguntseva, A. Hemmetter, A. Berestennikov, A. Pushkarev, A. Zakhidov, and Y. Kivshar, Adv. Opt. Mater. **7**, 1800784 (2019).
3. C. Perumal Veeramalai, S. Feng, X. Zhang, S. V. N. Pammi, V. Pecunia, and C. Li, Photonics Res. **9**, 968 (2021).
4. L. Protesescu, S. Yakunin, M. I. Bodnarchuk, F. Krieg, R. Caputo, C. H. Hendon, R. X. Yang, A. Walsh, and M. V. Kovalenko, Nano Lett. **15**, 3692 (2015).
5. L. Gu, K. Wen, Q. Peng, W. Huang, and J. Wang, Small **16**, 2001861 (2020).
6. S. Hussain, A. Raza, F. Saeed, A. Perveen, Y. Sikhai, N. Din, E. E. Elemike, Q. Huang, A. Subramanian, Q. Khan, and W. Lei, Chin. Opt. Lett. **19**, 030005 (2021).
7. M. Zheng and G. Fang, Nanoscale **13**, 16427 (2021).
8. C. Li, Z. Liu, Q. Shang, and Q. Zhang, Adv. Opt. Mater. **7**, 1900279 (2019).
9. Q. Shang, M. Li, L. Zhao, D. Chen, S. Zhang, S. Chen, P. Gao, C. Shen, J. Xing, G. Xing, B. Shen, X. Liu, and Q. Zhang, Nano Lett. **20**, 6636 (2020).
10. S. Cho, Y. Yang, M. Soljačić, and H. Yun Seok, Sci. Adv. **7**, eabf3362 (2021).
11. S. Zhang, Y. Zhong, F. Yang, Q. Cao, W. Du, J. Shi, and X. Liu, Photonics Res. **8**, A72 (2020).
12. G. Adamo, H. N. Swaha Krishnamoorthy, D. Cortecchia, B. Chaudhary, V. Nalla, N. I. Zheludev, and C. Soci, Nano Lett. **20**, 7906 (2020).
13. Z. Yang, M. Pelton, M. I. Bodnarchuk, M. V. Kovalenko, and E. Waks, Appl. Phys. Lett. **111**, 221104 (2017).
14. U. Stella, L. Boarino, N. De Leo, P. Munzert, and E. Descrovi, ACS Photonics **6**, 2073 (2019).
15. Y. Wu, Q. Han, M. Wang, F. Juan, G. Hou, F. Xun, H. Wei, J. Xu, and B. Cao, Opt. Express **29**, 36988 (2021).
16. J. Wang, R. Cao, P. Da, Y. Wang, T. Hu, L. Wu, J. Lu, X. Shen, F. Xu, G. Zheng, and Z. Chen, Appl. Phys. Lett. **108**, 022103 (2016).
17. S. Yang, W. Bao, X. Liu, J. Kim, R. Zhao, R. Ma, Y. Wang, and X. Zhang, Matter **4**, 4042 (2021).
18. J. T. Hugall, A. Singh, and N. F. van Hulst, ACS Photonics **5**, 43 (2018).
19. J.-E. Park, R. López-Arteaga, A. D. Sample, C. R. Cherqui, I. Spanopoulos, J. Guan, M. G. Kanatzidis, G. C. Schatz, E. A. Weiss, and T. W. Odom, ACS Nano **16**, 3917 (2022).
20. B. Li, H. Huang, G. Zhang, C. Yang, W. Guo, R. Chen, C. Qin, Y. Gao, V. P. Biju, A. L. Rogach, L. Xiao, and S. Jia, J. Phys. Chem. Lett. **9**, 6934 (2018).
21. J. Chen, Q. Zhang, J. Shi, S. Zhang, W. Du, Y. Mi, Q. Shang, P. Liu, X. Sui, X. Wu, R. Wang, B. Peng, H. Zhong, G. Xing, X. Qiu, T. C. Sum, and X. Liu, Commun. Phys. **2**, 80 (2019).
22. K. Wei, X. Zheng, X. Cheng, C. Shen, and T. Jiang, Adv. Opt. Mater. **4**, 1993 (2016).
23. P. Franceschini, L. Carletti, A. P. Pushkarev, F. Preda, A. Perri, A. Tognazzi, A. Ronchi, G. Ferrini, S. Pagliara, F. Banfi, D. Polli, G. Cerullo, C. De Angelis, S. V. Makarov, and C. Giannetti, ACS Nano **14**, 13602 (2020).
24. W. Du, J. Zhao, W. Zhao, S. Zhang, H. Xu, and Q. Xiong, ACS Photonics **6**, 2832 (2019).
25. M. Pelton, Nat. Photonics **9**, 427 (2015).